communications earth & environment

ARTICLE

https://doi.org/10.1038/s43247-022-00509-3 OPEN

Central Mediterranean rainfall varied with high northern latitude temperatures during the last deglaciation

Andrea Columbu [1,2]✉, Christoph Spötl [3], Jens Fohlmeister[4], Hsun-Ming Hu [5,6], Veronica Chiarini [7], John Hellstrom [8], Hai Cheng [9], Chuan-Chou Shen [5,6] & Jo De Waele [7]

Similarly to the effects of current climate change, the last deglaciation (Termination I) rapidly altered northern latitude temperatures and ice-sheet extent, as well as the Atlantic Meridional Overturning Circulation. However, it is still unclear how these changes propagated and impacted the central Mediterranean continental rainfall variability. This prevents a full understanding on how global warming will affect Mediterranean areas in the future. Here, we present a high-resolution reconstruction of rainfall changes in the central Mediterranean across Termination I, based on a novel $\delta^{18}O$ time series from a southern Italian stalagmite. Across Termination I the availability of Atlantic moisture varied in response to northern latitude temperature increases (decreases) and ice-sheet decreases (increases), promoting a higher (lower) intensity of the Atlantic Meridional Overturning Circulation, and resulting in a relatively wetter (drier) climate in the Mediterranean. In the light of future warming, this study emphasises the role of high-latitude climate changes in causing rainfall variation in highly populated Mediterranean areas.

[1] Department of Chemistry, Life Sciences and Environmental Sustainability. Earth Sciences Division, University of Parma, Parma, Italy. [2] Department of Earth Sciences, University of Pisa, Pisa, Italy. [3] Institute of Geology, University of Innsbruck, Innsbruck, Austria. [4] German Federal Office for Radiation Protection (BfS), Berlin, Germany. [5] High-Precision Mass Spectrometry and Environment Change Laboratory (HISPEC), Department of Geosciences, National Taiwan University, Taipei, Taiwan ROC. [6] Research Center for Future Earth, National Taiwan University, Taipei, Taiwan ROC. [7] Department of Biological, Geological and Environmental Sciences, University of Bologna, Bologna, Italy. [8] School of Earth Sciences, University of Melbourne, Melbourne, Australia. [9] Institute of Global Environmental Change, Xi'an Jiaotong University, Xi'an, China. ✉email: andrea.columbu2@gmail.com

Comprehending past rapid climate shifts is pivotal to evaluate the dynamics of current and future climate changes. As occurring today, during the last deglaciation (Termination I, T-I) global temperature[1,2] and greenhouse gas concentrations[3] rose rapidly, the sea level increased[4] as ice sheets retreated[5,6] and atmospheric and oceanic circulation patterns reorganised accordingly[7–9]. The final stages of T-I in Greenland, characterised not only by temperature increases but also by cooling events, lasted ~3.0 kyrs according to ice-core records[10]. After Greenland interstadial (GI) and stadial (GS) 2, a centennial[11,12], or even only decadal-scale[13,14] temperature increase (GI1) of around 10 °C starting at 14.64 ± 0.18 ka (ka = 10^3 years before 1950 C.E.)[15] was followed by a comparable temperature drop and a consequent return towards glacial-like conditions at 12.85 ± 0.14 ka (GS1). A centennial-scale ~10 °C warming finally led to the Holocene (11.65 ± 0.10 ka)[16]. These periods of Greenland climate instability preceding the Holocene, namely GI1 and GS1, occurred within the Bølling-Allerød (BA) and Younger Dryas (YD) chronozones respectively[15]. Uncovering how these abrupt northern high-latitude climate shifts were propagated to lower latitudes, and their pace and tempo at specific sites[17], is crucial to refine the understanding of the functioning of the intra-hemispherical climate dynamics on scales similar to the current climate change; thus, it helps to better assess the effect of the current warming of the Arctic on highly populated mid-latitude areas such as the Mediterranean region. The latter is a climate hotspot[18], and consequences on the environment and economy of this region will be particularly pronounced. Extreme storms[19,20] have already resulted in flooding in the last decade, where Mediterranean cities such as Bari (2005), Vicenza (2010), Genoa (2011, 2014), Nice (2015), Mallorca (2018), Palermo (2020), Como (2021) and Catania (2021) had numerous casualties. Summer heatwaves coupled with dryness are even more often impacting local economies[21].

Recent studies have sensibly improved the T-I continental chronology in the Mediterranean[17], but precisely dated terrestrial archives are largely confined to the western and eastern sides of the basin[17,22–24], while they are scarce and/or fragmentary in the central portion. Here, speleothem-based reconstructions of T-I are virtually absent[25], and paleo-data are largely derived from lacustrine records only[26,27]. As a result, multi-archive information about the impact of T-I on important components of in-land climate, as for example rainfall, are unavailable for large parts of the Mediterranean.

One such area is Italy, which is strategically located for the study of the central Mediterranean climate. Italy's present-day climate is governed by the westerlies, which transport moisture from the Atlantic and modulate temperature[28], thus having a major impact on agriculture and ecosystems[29]. The availability of Atlantic moisture and the strength of the westerlies in delivering moisture across the Mediterranean change on glacial-interglacial timescales, in relation to the ice-sheet extent in the northern high latitudes[30]. The Atlantic Meridional Overturning Circulation (AMOC) is weaker and the northern ice front moves southward during glacials[31]; lower temperatures reduce evaporation from the surface of the Atlantic and limit the advection of moisture towards the Mediterranean[32], leading to a drier climate. The westerlies and the AMOC, besides controlling hydroclimate dynamics in Mediterranean regions close to the Atlantic coast[24], also have a far-reaching impact on the climate further to the east, by for example influencing the hydroclimate and monsoonal activity in the Middle East and Asia, respectively[22,33]. Deglaciations reverse the above-mentioned situation and, during T-I, the greater availability of Atlantic moisture and stronger westerlies resulted in increased rainfall in the Mediterranean region[34], as also suggested for the preceding deglaciation[32]. Cyclogenesis also occurs in the Mediterranean realm[35], and this might predominate when the advection of Atlantic moisture is limited[36]. Stronger Mediterranean cyclogenesis is expected during times of reduced westerly air flow. These processes have been documented for the western side of the basin for the last ~35 ka[24,37,38] as well as for some older periods[39,40]. For the central Mediterranean, however, rainfall dynamics across T-I remain largely underexplored. Studies of lacustrine sediments did not specifically examine T-I[26,27,30] and speleothem-based reconstructions are only available for older periods[36]. Tightly constraining the timing and progression of T-I in the central Mediterranean and its associated rainfall dynamics is the goal of this paper. This is accomplished by using a high-resolution palaeoclimate reconstruction based on a stalagmite (SA1) from southern Italy (Sant'Angelo Cave, Apulia). Oxygen stable isotope ($\delta^{18}O$) time series is used to 1) accurately constrain the timing of the hydroclimate across T-I, and (2) to evaluate the impact of GI1, GS1 and the early Holocene, as well as other associated events especially in terms of rainfall variability. By doing so, this work ascertains the role of the westerlies in controlling central Mediterranean rainfall dynamics during the largest climate change in recent Earth's history, with implications for a better understanding of regional hydroclimate changes in this region related to current global warming.

Results and discussion

SA1 stalagmite. SA1 is a ~30 cm-long calcite stalagmite sampled in Sant'Angelo Cave (40.73° N, 17.57° E, Fig. 1, Supplementary Fig. 1 and methods). The age-depth model[41] based on high-resolution U-Th dating (total $n = 36$, period of interest $n = 24$, methods) attests its deposition between $47.8^{+0.41}/_{-0.39}$ and $6.63^{+0.62}/_{-0.57}$ ka (Fig. 1). $\delta^{18}O$ analyses (total $n = 1045$; period of interest $n = 546$, methods) result in an average resolution of 28 years during the period of interest (from ~25 to ~10 ka), and average uncertainties of ±0.30 kyrs (Fig. 1 and Supplementary Fig. 2).

Rainfall variability during T-I. Several lines of evidence point to the primary role of the amount and source effects[42] in controlling SA1-$\delta^{18}O$ (methods). SA1-$\delta^{18}O$ is thus here taken as a rainfall proxy, with more negative values representing wetter periods with a major contribution of Atlantic-derived rainfall. Less negative values are instead suggesting drier periods with a higher contribution of Mediterranean-derived moisture. The same pattern is found in past[24,37] and modern[43] rainfall dynamics on the western side of the Mediterranean basin. From the late glacial to the Holocene, SA1-$\delta^{18}O$ and Greenland ice cores[10] show overall similar trends (Fig. 2). This high degree of similarity implies that the central Mediterranean climate changed in concert with temperature and ice-sheet extent variations at high latitudes, as also testified by other studies on the Atlantic fringe of northern Iberia[44]. In the study area, these variations triggered changes in rainfall amount and source. Similar to older periods[32,36,45], low temperatures of the North Atlantic and northern ice-sheet advances caused relative aridity in the central Mediterranean, while glacial retreats and higher temperatures led to an increase in precipitation. Concurrently, wetter periods in the study area entail a higher proportion of Atlantic-sourced humidity, whereas drier intervals feature a higher percentage of moisture originated within the Mediterranean basin.

Ice-core data show that GI2 was composed of two rapid warmings (GI2.2 and GI2.1) starting at 23.34 ± 0.60 and 23.02 ± 0.58 ka respectively, while GS2.1a started at 17.48 ± 0.33 and peaked at 16.05 ± 0.20 ka[15]. SA1 registered an increase in rainfall (and a higher ratio of Atlantic vs. Mediterranean-sourced humidity) at the onset of the Mediterranean equivalent of GI2.1 at $23.16^{+0.19}/_{-0.19}$ ka, as shown by the shift towards more

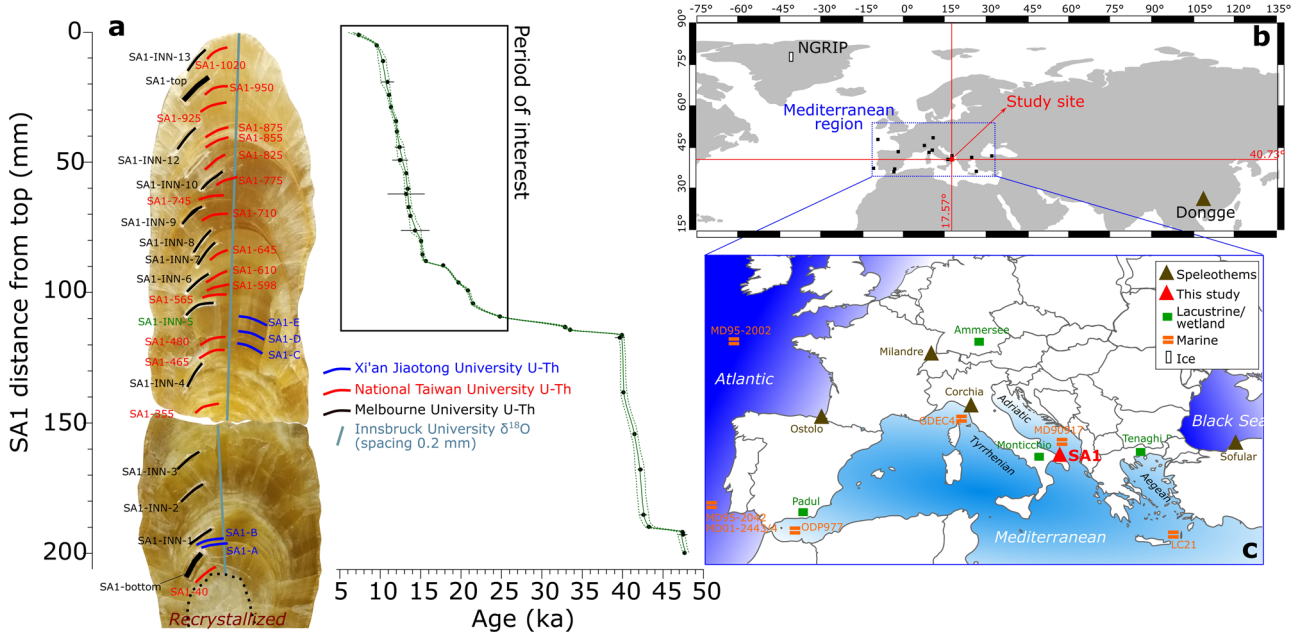

Fig. 1 Sample, analyses and study site. a SA1 stalagmite and analyses accomplished in this study. Coloured bars refer to U-Th dating at Xi'an Jiaotong (blue), National Taiwan (red) and Melbourne (black) Universities, while the blue line marks $\delta^{18}O$ analyses (methods) carried out at Innsbruck University. The age model is reported with dots and 2σ error bars (indicating the U-Th ages) and their relative interpolation (green line = average model; dotted lines = propagation of ±2σ uncertainties). **b**, **c** Study site and other records discussed in the text.

negative values of $\delta^{18}O$ (Fig. 2); instead, from 17.74 $^{+0.11}/_{-0.12}$ ka SA1-$\delta^{18}O$ demonstrates a period of less negative values reflecting a decrease in rainfall amount (and a reduced ratio of Atlantic vs. Mediterranean-sourced humidity - Fig. 2). This culminates with a very dry interval between 16.53$^{+0.10}/_{-0.11}$ and 16.04$^{+0.11}/_{-0.12}$ ka, synchronous with the peak of GS2.1a in Greenland (Fig. 2). The latter driest interval, lasting ca. 500 years, is associated with Heinrich Stadial 1 (HS1)[46], which marked a drop in temperature in northern Iberia[44] (Fig. 3) and resulted in record-dry conditions in southern Iberia[24]. The timing of the transition into GI1 in the NGRIP record and its equivalent in SA1 is consistent, although showing a different pattern. NGRIP records a first gradual increase in temperature (red arrow in Fig. 2) starting at 16.05 ± 0.2 ka, followed by a rapid shift at 14.64 ± 0.18 ka leading to GI1. SA1 instead captured a step-like increase in rainfall (and an increase in the ratio of Atlantic/Mediterranean-sourced humidity) starting at 16.04$^{+0.11}/_{-0.12}$ ka, with a first rapid pulse leading to a more stable period (step 1 in Fig. 2), from 15.53$^{+0.16}/_{-0.14}$ to 14.04$^{+0.46}/_{-0.42}$ ka. This centennial-scale increase coincided with increased rainfall in southern Iberia[24] (black arrow in Fig. 1). Step 1 was followed by a second increase in rainfall (step 2 in Fig. 2) starting at 14.04$^{+0.46}/_{-0.42}$ ka and marking the inception of the equivalent of GI1; the latter terminated at 13.02$^{+0.31}/_{-0.30}$, consistent within uncertainties with the Greenland ice-core records (12.85 ± 0.14 ka). The end of the GI1 marks the beginning of GS1, a return to near-glacial conditions in Greenland until 11.65 ± 0.1 ka. The equivalent of GS1 in the study area was characterised by a dry climate (and a reduced ratio of Atlantic/Mediterranean-sourced humidity) in the central Mediterranean according to SA1, terminating at 11.95 $^{+0.15}/_{-0.19}$ ka. The southern Iberian rainfall index[24] records a drier climate during this period (Fig. 2). The start of the Holocene entailed a rapid warming in Greenland and an associated increase in rainfall in southern Iberia and in the study area (Fig. 2). Accordingly, SA1 suggests a first precise constraint for the lower boundary of the Holocene in the central Mediterranean (11.95 $^{+0.15}/_{-0.19}$ ka), which needs to be confirmed by future studies targeting terrestrial proxies in the same region. The link between western and central Mediterranean rainfall variability is further constrained at intra-Holocene timescales (blue double-arrow in Fig. 2). Indeed, from 10.51 $^{+0.41}/_{-0.43}$ to 9.60 $^{+0.16}/_{-0.14}$ ka SA1 records a relatively dry period that has a counterpart in southern Iberia[24].

Controls on Mediterranean climate across T-I. Growth of SA1 between 47.82$^{+0.41}/_{-0.39}$ and 6.63$^{+0.62}/_{-0.57}$ ka, and of the PC stalagmite[36] (from Pozzo Cucù cave, located 40 km northwest of SA) from 106.02$^{+2.8}/_{-2.7}$ to 26.6$^{+0.8}/_{-0.9}$ ka, demonstrates that (1) rainfall in southern Italy efficiently recharged the karst aquifers even during the peak of the last glacial; and (2) coupled with the availability of moisture, temperatures were never too low to impede vegetation and soil bioproductivity, hence allowing speleothem deposition in these caves. Precipitation minus evaporation (P-E) was thus positive during the SA1 and PC growth periods, and the widespread aridity and low temperatures affecting central Europe, leading to growth stops in speleothems progressing towards the last glacial acme[25], were apparently less severe in the central Mediterranean region. This agrees with observations from the eastern side of the basin[22,23], where speleothems grew continuously across the last glacial period. However, as registered by SA1-$\delta^{18}O$, rainfall fluctuated across T-I (Figs. 2 and 3 and methods), but recharge of karst aquifers and related speleothem deposition did not cease even during relatively dry periods. These variations overall agree with Greenland GI/GS2, GI/GS1, and the Holocene inception (Fig. 2), and are also comparable with equivalent rapid climate shifts occurring in continental southern Iberia[24]. Along a west-to-east transect across the Mediterranean, this pattern of T-I climate variability is also seen in planktonic foraminifera $\delta^{18}O$ data of core ODP977 from the Spanish Margin[47], core GDEC-4-2 from the Tyrrhenian Sea[48], as well as from the Aegean Sea[49] (LC21 core) (Fig. 3). This shows that SA1 captured the regional climate variability rather than local cave-related processes. Sea-surface temperatures (SST) changed accordingly on the Portugal Margin[50] (MD95-2042 core)

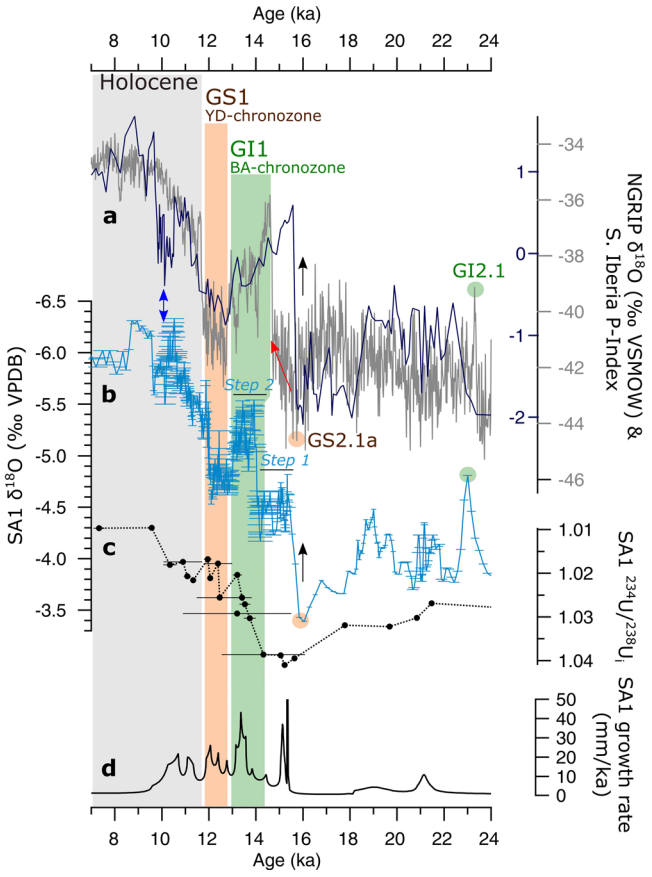

Fig. 2 SA1 hydroclimate proxies compared to Greenland ice-core data and the Iberian precipitation index. a $\delta^{18}O$ Greenland ice-core time series (grey line[10]) with highlighted GI1 (BA-chronozone), GS1 (YD-chronozone) and Holocene, together with the precipitation index (P-Index) from southern Iberia (blue line[24]). **b** SA1 $\delta^{18}O$ time series with age uncertainty error bars. **c** SA1 initial $^{234}U/^{238}U$ activity ratio and **d**) growth rate. Peaks of GI2.1 and GS2.1a are marked with a green and pink circle, respectively. The red arrow indicates the gradual warming after peak GS2.1a conditions in Greenland. The black arrows highlight the rapid rainfall variation in the study site and northern Iberia after the same event. Steps 1 and 2 indicate the progression toward GI1 captured in SA1 (see text). The blue double-arrow shows an intra-Holocene dry interval recorded by both SA1 and the P-Index.

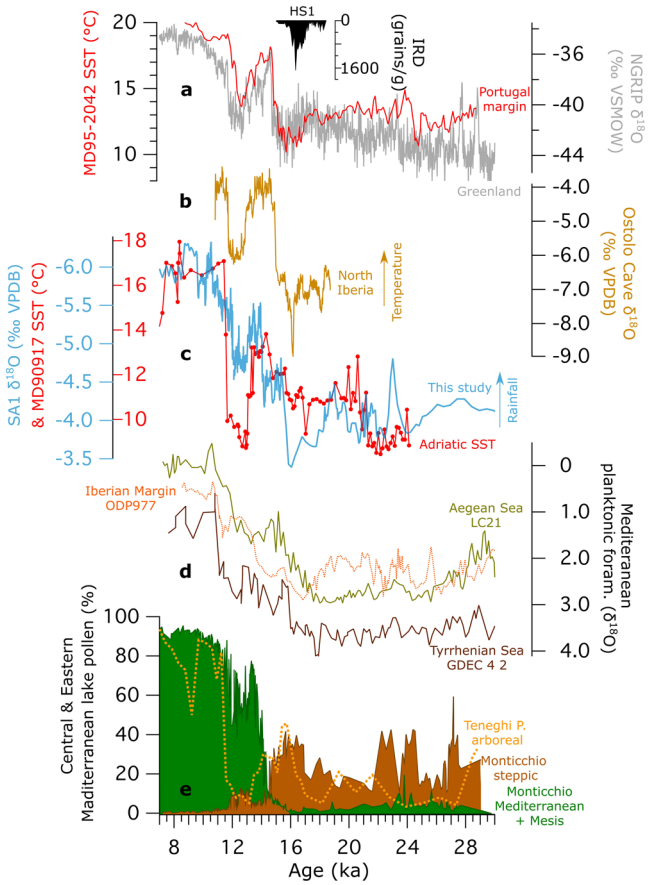

Fig. 3 SA1 $\delta^{18}O$ time series compared to circum-Mediterranean records. **a** Ice rafted debris (IRD) from the Gulf of Biscay related to the HS1 event (black fill[47]), Portugal Margin SST (red line[50]) and Greenland ice-core $\delta^{18}O$ (grey line[10]). **b** Ostolo Cave stalagmite $\delta^{18}O$, a proxy for northern Iberian temperature (yellow line[44]). **c** SA1 $\delta^{18}O$ (light blue line, this study) taken as palaeo-rainfall proxy and Adriatic SST (red line[51]). **d** Planktonic foraminifera from the Aegean Sea (brown line[49]), the Tyrrhenian Sea (purple line[48]) and the Iberian Margin (dotted orange line[46]), proxies for Mediterranean planktonic-derived temperatures. **e** Pollen from Monticchio (green and brown fill[26]) and Tenaghi Philippon lakes (yellow dotted line[27]), representing vegetation changes. For locations see Fig. 1.

and in the Adriatic Sea[51], as well as in continental western (Ostolo Cave[44]) and central (Milandre Cave[52]) Europe (Fig. 3 and Supplementary Fig. 3). For example, air temperatures increased ~6 °C at the GS1-Holocene transition in Switzerland[52] (Supplementary Fig. 3), synchronous with the equivalent transition captured is SA1. Lacustrine ostracod $\delta^{18}O$ data from Ammersee in southern Germany agree with this temperature shift[53] (Supplementary Fig. 3), while pollen from southern Italy (Monticchio Lake[26]) and Greece (Tenaghi Philippon Lake[27]), although of low resolution, testify the expansion of trees and Mediterranean taxa during the equivalent of GI1 and the GS1-Holocene transition (Fig. 3). Especially during the peak of GS2.1a and to a smaller extent during GS1, the reduction in the arboreal pollen was accompanied by the expansion of steppe environments in the Monticchio Lake area[26]. The latter lake is located in the southern Apennine chain (656 m a.s.l.) ca. 170 km west of the study site, with a maximum catchment elevation of 956 m a.s.l. This implies that the local ecosystem at Monticchio responded to the same rainfall variability across T-I, likely coupled with temperature changes, also captured by SA1. As recently demonstrated, the reorganisation of the northern hemisphere (hydro)climate during T-I occurred within a few decades in response to temperature and ice-sheet extent changes in the Arctic[54]. It impacted not only the climate in central Europe and the Mediterranean, but also the hydroclimate in the Middle East[23] and the monsoon activity in Asia[33] (Supplementary Fig. 3).

Our data suggest a rapid variability of the westerly moisture advection across T-I in the central Mediterranean area. A similar reorganisation of the atmospheric circulation has been proposed for the western side of the basin[24], suggesting that the entire western and central Mediterranean responded in a coherent manner to Atlantic and northern latitude climate forcings. Indeed, the westerly moisture advection toward the Mediterranean reached its lowest intensity during the equivalent of GS2.1a (Fig. 4). The period of lowest westerlies intensity lasted for ca. 500 years between $16.53^{+0.10}/_{-0.11}$ and $16.04^{+0.11}/_{-0.12}$ ka, when HS1 induced minimum temperatures as testified by records from the Bay of Biscay (MD95-2002 core[46]), Northern Iberia (Ostolo Cave[44]) and the Adriatic (MD90917 core[51]) (Figs. 1 and 3). The related weakened AMOC triggered a period of record-low rainfall in the central Mediterranean. Because of the reduced availability

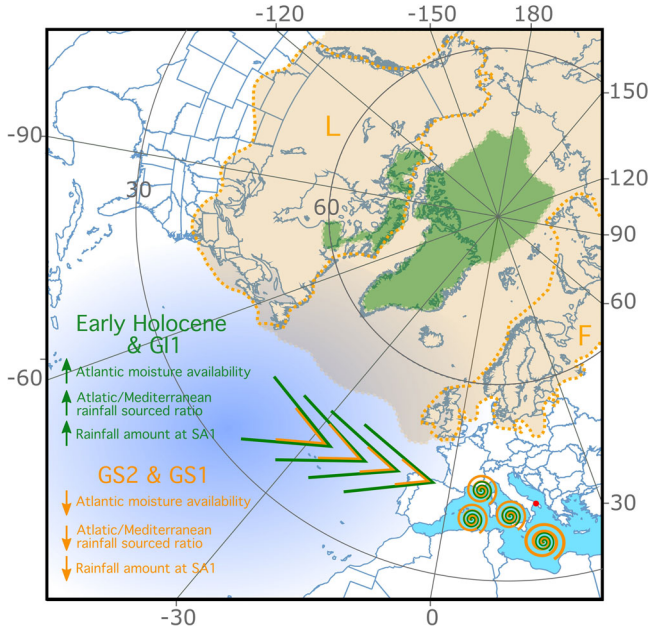

Fig. 4 Controls on central Mediterranean rainfall during T-I. Extension of Holocene and GI1 northern ice (green shading) compared to GS2 and GS1 (orange shading). The extent of the Greenland, Laurentide (L) and Fennoscandian (F) ice sheets is shown by dotted lines. The two main moisture sources for the study area (red dot) are marked by open triangles and spirals during the Early Holocene and GI1 (green) and GS1 and GS2 (orange), with their size proportional to their importance. During GS1 and GS2, northern ice sheets expanded, global temperatures decreased and the AMOC weakened. This reduced the westerly moisture advection into the central Mediterranean, where rainfall was mainly derived from Mediterranean cyclogenesis (orange spirals). In the central Mediterranean (study area), the rainfall amount dropped accordingly. During GI1 and the Early Holocene, the northern ice sheets retreated, regional temperatures increased and the AMOC became stronger. The higher availability of Atlantic moisture and increased advection across the Mediterranean Sea led to higher rainfall in the central part of the basin, while Mediterranean cyclogenesis played only a minor role in the study site, similar to modern conditions (see Supplementary Fig. 4).

of Atlantic-sourced moisture in colder-than-today periods, likely partially sourced from the subtropical moisture reservoir[55], karst aquifer recharge at SA1 was possibly sustained by Mediterranean-sourced rainfall (methods). At this time, the Atlantic/Mediterranean-sourced rainfall ratio reached its lowest value within the period of interest. Additionally, low air temperatures in the study area[51] played a role in maintaining P-E > 0.

The transition toward the equivalent of GI1 in SA1 shows a step-like pattern (Fig. 2). A similar pattern was recorded by Adriatic SST[51] and, albeit of lower resolution, by Iberian Margin[47] planktonic foraminifera $\delta^{18}O$ (Fig. 3). We propose that rainfall in central-south Italy rapidly increased at $15.53^{+0.16}/_{-0.14}$ in concert with the western side of the basin[24] (black arrow in Fig. 2), while Greenland was gradually warming (red arrow in Fig. 2) and the AMOC was strengthening with respect to GS2.1a (Fig. 4). However, during the phase called step 1 (Fig. 2), Mediterranean cyclogenesis in the study area was possibly still influencing the rainfall, as the same step-like pattern was not found in Iberia[24]. The latter, situated between the Atlantic and southern Italy, recorded a higher sensibility to the Atlantic-dominated hydroclimate dynamics than the study site, during a phase of gradual temperature increase in Greenland and a reorganisation of the atmospheric circulation. It is thus possible that the westerlies were delivering moisture to southern Iberia, but their strength was not sufficient to overcome the Apennine mountain belt, giving rise to a rain shadow effect in the study site (Supplementary Fig. 1), However, the rapid GI1-related warming in Greenland at 14.64 ± 0.18 ka was associated with a strengthening of the westerlies delivering moisture to the study site (Fig. 4). Accordingly, this warming resulted in a net increase in rainfall in the study site from $14.04^{+0.46}/_{-0.42}$ to $13.02^{+0.31}/_{-0.30}$ ka during the equivalent of GI1, testifying the northern latitude control on central Mediterranean rainfall over this (and the following) period. Indeed, GI1 ended at 12.85 ± 0.14 ka in Greenland and temperatures in the Adriatic, Portugal and on the Iberian Margin, as well as in northern Iberia, dropped accordingly (Figs. 2 and 3) because of the establishment of the GS1, which in Greenland terminated at 11.65 ± 0.1 ka. SA1 records a consistent period of low rainfall amount from $13.02^{+0.31}/_{-0.30}$ to $11.95\ ^{+0.15}/_{-0.19}$ ka, which was associated with reduced Atlantic evaporation and weak westerly moisture transport (and GI1, Fig. 4) that also led to a synchronous rainfall reduction in southern Iberia[24] (Fig. 2). Because temperatures in the Adriatic dropped by at least 5 °C during the equivalent of the GI/GS1 transition (Fig. 3), with values even lower than those before GI1[(51)], Mediterranean-sourced moisture was not able to counterbalance the Atlantic-derived moisture deficit. Thus, during GS1, the Atlantic/Mediterranean-sourced rainfall ratio was intermediate between the lowest values reached during the peak of GS2.1a and the highest values reached during the Early Holocene (see below). Finally, the onset of the Holocene in Greenland (11.65 ± 0.1 ka) was characterised by a rapid warming and a decrease in ice-sheet extent. The AMOC rapidly returned to its interglacial mode, resulting in a high availability of Atlantic moisture and its efficient westerly advection across the Mediterranean. In the study site, the Holocene started at $11.95\ ^{+0.15}/_{-0.19}$ ka testified by an increase in rainfall amount (Figs. 2 and 3), also reported from southern Iberia[24] (Fig. 2). Today the majority of rainfall in the central Mediterranean is related to the westerlies[28,35] (Fig. 4 and Supplementary Fig. 4), and Mediterranean-sourced moisture plays only a minor role. The Atlantic/Mediterranean-derived rainfall ratio was possibly even higher during the Early Holocene, as suggested by studies on the western side of the Mediterranean basin[24,37,38]. Therefore, the beginning of the Holocene in the study area led to the resumption of strong westerlies, transporting moisture towards the central Mediterranean, with the Atlantic/Mediterranean-sourced rainfall ratio reaching maximum values. Analogous to quantitative rainfall reconstructions in southern Iberia[56], SA1 attests that the westerly-driven rainfall variability found across T-I was mostly related to changes in winter rainfall amount (Supplementary Fig. 5). This should be taken into account in models aiming to assess future rainfall patterns in the central Mediterranean in response to the ongoing warming of the Arctic.

Conclusions

This study provides, for the first time, a robust speleothem-based chronology for the T-I related events (i.e., the GI/GS variability) and Holocene inception in the central Mediterranean. Atmospheric and oceanographic oscillations in the high northern latitudes during T-I led to changes in moisture sources and rainfall amount. These changes occurred in response to a reduced availability of Atlantic moisture and a weakened westerly moisture transport across the Mediterranean during periods of weak AMOC (GS1 and 2). In the central Mediterranean, this led to a pronounced decrease in rainfall amount as well as of the Atlantic/Mediterranean-sourced rainfall ratio. Conversely, Atlantic moisture availability and westerly advection increased at times of strong AMOC (GI1 and Early Holocene), resulting in an increase

in rainfall in the central Mediterranean climate as well as of the Atlantic/Mediterranean-sourced rainfall ratio. In the Mediterranean, modern rainfall mostly occurs in winter and autumn (methods), while spring and especially summer are typically dry. Heavy storms[19,20] are increasingly procuring flooding in highly populated areas of the Italian Peninsula, mostly occurring during winter and autumn. Together with summer heat waves, current climate change is increasingly causing economic losses (i.e., 40 and 25% reduction in fodder and maize respectively because of the summer 2003 heatwave[21]). Such weather extremes will possibly intensify according to future climate scenarios[57]. Our research documents that rainfall variability in the central Mediterranean during T-I can be linked to events occurring at high northern latitudes. This study reaffirms the role of Atlantic moisture in procuring high rainfall in the central Mediterranean during high-magnitude warming events that characterised the end of the last glacial period.

Methods

Area of study and stalagmite. Apulia hosts one of the largest karst areas in Italy, with more than 2000 caves. The study cave belongs to the Apulian carbonate foreland platform, which is a poorly deformed low-altitude plateau stretching NW-SE for over 100 km, between the southern Apennine foothills and the coastline. Sant'Angelo cave (40.73°N, 17.57°E) is located in the municipality of Ostuni, ~6 km from the Adriatic coastline (Fig. 1 and Supplementary Fig. 1). It is carved in Cretaceous limestone of the Calcare di Altamura Formation, with an entrance at 148 m a.s.l. and comprising a subhorizontal tunnel of 250 m length. The thickness of overlying rock is between 20 and 40 m. The study area is characterised by a meso-thermo Mediterranean sub-humid climate. We refer to meteorological data from the city of Ostuni (last 60 years), the closest available station (<5 km from the cave entrance) of the Italian Protezione Civile service. Average annual precipitation is 699 mm, with November and July being the wettest (93 mm/y) and driest (16 mm/y) months, respectively. January (min: 5.8 °C, max: 11.0 °C, average: 8.4 °C) and August (min: 21 °C, max: 29.1 °C, average: 25.0 °C) are the coldest and warmest months, respectively (Fig. Sup. 4). Annual average temperature is 16.4 °C (min: 13.0 °C, max: 19.9 °C) The majority of precipitation is due to westerly-driven air masses, whose sources are located in the Atlantic, and wind direction is from north-west. Secondary sources are the Mediterranean basin itself and the Euroasian landmass (Supplementary Fig. 4). SA1 stalagmite was found broken close to its original growth position. It is ~30 cm tall, yellowish/translucent in most of its parts and shows macroscopic layering over most of its length. It widens ~9 cm from the bottom and then shows a regular candle-shape morphology with a diameter of ~8 cm. The bottom 9 cm show evidence of diagenesis (dissolution and reprecipitation) and have therefore been excluded from the analyses (Fig. 1).

U-Th dating, age model and $\delta^{18}O$ analyses. Powdered subsamples ($n = 36$) weighing ~50 to ~100 mg were obtained from SA1 by using a manual drill with a 1 mm diameter drill bit (Fig. 1 for locations). These subsamples were extracted perpendicular with respect to the growth axis and forming narrow and elongated trenches following as much as possible the speleothem lamination. U-Th dating analyses were performed in the High-Precision Mass Spectrometry and Environment Change Laboratory of the National Taiwan University (Taiwan) ($n = 18$), in the School of Earth Sciences of the University of Melbourne (Australia) ($n = 14$), and at the Institute of Global Environmental Change of Xi'an Jiaotong University (China) ($n = 5$). For the period considered in this study, from ~25 to ~10 ka, a total of 24 U-Th ages were produced. Briefly, the preparation of the samples involved dissolving calcite in HNO_3, separating U and Th compounds through decontaminated resin ion-exchange columns and spiking by a solution of known $^{229}Th/^{233}U/\ ^{236}U$ ratio. The obtained solutions were then analysed using a multi-collector inductively coupled plasma mass spectrometer (MC-ICP-MS). The standard chemical and instrumental procedures applied in the three institutions, as well as the methods used for the correction of the raw data, are detailed elsewhere: Xi'an Jiaotong[54], Melbourne[58] and Taiwan[59]. Half-lives of nuclides used for age calculation are given elsewhere[54]. The age-depth model was constructed using the COPRA algorithm[41], which provides ages and propagated uncertainties.

For $\delta^{18}O$, SA1 was milled at 0.2 mm spacing along the central growth axis (drill bit diameter 0.2 mm), and ~0.1 mg of the resulting powder was prepared in a continuous-flow system (GasBench II) and were then measured in a ThermoFisher Delta V plus mass spectrometer at the Institute of Geology, University of Innsbruck (Austria). NBS18, NBS19, CO1, and CO8 standards were used as references. The results are expressed in per mil (‰) units relative to the Vienna Pee Dee Belemnite (VPDB) standard. The 1σ analytical reproducibility was ±0.08‰ for $\delta^{18}O$. SA1 $\delta^{18}O$ results (total $n = 1045$; period of interest $n = 546$) were anchored to the age-depth model to create the time series interpreted in this paper.

Transition detection algorithm. The stadial-interstadial transitions of stalagmites PC[36] and SA1 (this study) during Dansgaard/Oeschger (DO) cycles were detected via an automated approach (Supplementary Fig. 6). Two neighbouring running windows (window length = 200 years) on the annually interpolated stalagmite $\delta^{18}O$ data were used. The maximum difference of the average of both sliding windows indicates periods of fast $\delta^{18}O$ changes in the data. As stadials show less depleted values compared to interstadials in both speleothems, local minima are the best candidates for a stadial-interstadial transition. In order to find corresponding interstadials in the speleothem data and the Greenland ice cores the stadial-interstadial transitions as established in the NGRIP $\delta^{18}O$ record[10] on its GICC05modelext time scale[15] are used as a reference. The method analyses only those local maxima of the differences of the average of both windows which are in a narrow temporal vicinity with respect to the start of interstadials as defined by NGRIP[15]. For an individual NGRIP defined stadial-interstadial transition, the time period in which the transition of the stalagmite shall be attributed, is defined to be as large as the half-length of the duration between the stadial-interstadial transition and the next nearest one. We widened this range by the 2σ uncertainty of the U-Th chronology of the respective time period for individual stadial-interstadial transitions. If the age difference between two corresponding stadial-interstadial transitions in both archives was too far off, no DO event was detected. Another limiting factor was the maximum difference between both window averages, which must be large enough to be accounted for. Here, the standard deviation of the differences of both sliding windows was applied as a threshold; local maxima must be larger than the standard deviation of the difference curve of both sliding windows to be considered as an event.

Results. All U-Th ages are in stratigraphic order within uncertainties (Supplementary Data 1). Concentration of ^{238}U is on average 303 ppb (min: 130 ppb; max: 600 ppb), while the detrital thorium is minimal, considering that the average $^{230}Th/^{232}Th$ activity ratio is well above 1000 (min: 10; max: 11030). For these reasons, the resulting age uncertainties are small (min: 0.3%; average: 2%; max: 17%). According to the COPRA age model, SA1 grew from $47.8^{+0.41}/_{-0.39}$ to $6.63^{+0.62}/_{-0.57}$ ka; the period of interest for this study spans from $24.80^{+0.23}/_{-0.25}$ to $9.57^{+0.16}/_{-0.15}$ ka, with average chronological uncertainties of ±0.30 kyrs. SA1 $[^{234}U/^{238}U]_i$ varies through time (Fig. 2); from values of around 1.025 at around the peak of GI2.1, it then shifts toward the maximum values (above 1.04) at around the peak of GS2.1a ($16.04^{+0.11}/_{-0.12}$ ka); afterwards the values monotonously decrease toward the Holocene and reaching the minimal values (1.01) at $9.57^{+0.16}/_{-0.15}$ ka. The average growth rate is 15.4 mm/ka during the period of interest (Fig. 2). Between ~25 to 16 ka values are always below 10 mm/ka (Fig. 2), reaching minimal values at $16.04^{+0.11}/_{-0.12}$ ka (~0.8 mm/ka). Just after $16.04^{+0.11}/_{-0.12}$ ka, growth rate demonstrates the first peak, rapidly reaching (and exceeding) ~50 mm/ka. Then, a period of decreased growth rate with values around ~10 mm/ka coinciding with the step 1 of the progression toward the equivalent of GI1 (Fig. 2) is followed by a second peak of high growth rates (~40 mm/ka) during the equivalent of GI1 at $13.36^{+0.35}/_{-0.36}$ ka. Afterwards, values decrease again reaching ~26 mm/ka during the equivalent of GS1 at $12.05^{+0.14}/_{-0.13}$ ka. During the first part of the Holocene and until ~10 ka, growth rate remained around 20 mm/ka, while lower values occur after ~10 ka towards the top of the stalagmite.

During the period of interest the resolution for SA1-$\delta^{18}O$ is 28 years. The values oscillate between −3.4 and −6.3 ‰, while its pattern resembles the NGRIP ice-core record[10] but showing an inverse correlation: more negative $\delta^{18}O$ values of SA1 are associated with less negative NGRIP $\delta^{18}O$ and vice versa. These similarities, together with the palaeoclimate significance of SA1-$\delta^{18}O$ (see below), allowed to identify the main climate periods considered within this work: GI/GS 2, GI1/GS 1 and the early Holocene inception (Fig. 2). As these periods in SA1-$\delta^{18}O$ are characterised by abrupt shifts, we took the ages of the $\delta^{18}O$ values at the midpoint of the transitions to assign base and top ages for two contiguous events. For example, at around ~12 ka SA1-$\delta^{18}O$ shifts from −4.5 to −5.7 ‰ in less than 300 years; the midpoint of this transition at 11.95 $^{+0.15}/_{-0.19}$ ka is considered as the onset of the Holocene. The same approach was applied to the equivalents of GI1 and GS1. The peaks of equivalents of GI2.1 and GS2.1a were identified by minima and maxima in SA1-$\delta^{18}O$ values an at $23.00^{+0.18}/_{-0.20}$ ka and $16.04^{+0.11}/_{-0.12}$ ka, respectively.

Finally, the transition detection algorithm was used to identify the equivalents of DOs 12, 11, 10, 9, 7, 6, 3 and 2 in SA1-$\delta^{18}O$. This also allowed to identify that the transitions into DO 12, 11, 10, 9, 7 6, 3 occurred synchronously, within uncertainties, in PC and SA1.

Proxy interpretation. The resemblance of SA1 time series with the NGRIP curve and other records presented in the text is already a strong indication that SA1-$\delta^{18}O$ reflects surface-related events rather than karst processes. Indeed, if calcite was deposited under non-equilibrium conditions[60], kinetic processes would have dominated $\delta^{18}O$ fractionation, concealing the original isotopic signature. This is well known[61] and different methods are usually applied to test whether or not stalagmites were deposited under equilibrium conditions. Here, SA1-$\delta^{18}O$ is compared to PC-$\delta^{18}O$, a stalagmite from a cave of the same area of SA1[36], thus procuring a replication test[62] for the period between ~48 and ~27 ka. Indeed, if the $\delta^{18}O$ of two stalagmites from the same cave/area replicate, this means they were responding to the same (external) climate signal trigger rather than to local

karst-related factors. SA1 and PC overlap between ~48 and ~27 ka (Supplementary Fig. 6), and their $\delta^{18}O$ time series show a high degree of reproducibility. In terms of absolute values they both oscillate between −4‰ and −6‰. Within age uncertainties their $\delta^{18}O$ pattern mostly agrees. Taking in consideration DO cycles found in Columbu et al. (2020)[36], SA1 and PC replicate DOs 12, 11, 10, 9, 7, 6 and 3 well. This correlation was rigidly constrained by using the transition detection method, applied to both SA1 and PC $\delta^{18}O$ time series (Supplementary Fig. 6). At the same time, $\delta^{18}O$ in SA1 and PC show divergences during the overlapping period (Supplementary Fig. 6). The two cave sites are dominated by similar climate today (in terms of temperature and rainfall, see Supplementary Fig. 4), and the topographic/geographic setting is also comparable (Supplementary Fig. 1). Thus, the observed divergences might be related to 1) the different resolution of the two records, and 2) heterogeneities of the two karst systems, influencing the $\delta^{18}O$ signature of the stalagmites. Interestingly, SA1-PC $[^{234/238}U]_i$ and growth rate (Supplementary Fig. 6) are also similar within the overlapping section, suggesting that the two karst systems were also responding to the same climate drivers in terms of (i) residence time; and (ii) cave dripping and $CaCO_3$ supersaturation (see later). Therefore, if the replication test attests that SA1 was deposited under equilibrium conditions from ~48 to ~27 ka, it is reasonable to think that the younger portion (the target of this study) has the same characteristics. However, it is known that carbonates[63], including stalagmites[64] never form under full equilibrium conditions, although caves are conservative environments where processes favouring kinetics (i.e., evaporation, rapid CO_2 degassing, etc.) are commonly limited[65]. For this reason, a small influence of kinetic fractionation in SA1-$\delta^{18}O$ cannot be excluded and, similar to our previous studies[36,45,66,67], SA1 is considered as having been deposited under quasi-equilibrium conditions. The replication test also rules out peculiar in-karst processes as main factors driving SA1-$\delta^{18}O$. Accordingly, SA1-$\delta^{18}O$ variations primarily reflect palaeoclimate/palaeo-environmental changes. Finally, post-depositional diagenetic processes such as calcite dissolution/redeposition can compromise the original geochemical composition of the stalagmite[68]. However, SA1 does not show any visual evidence of recrystallization in the studied section (i.e., above the dotted line in Fig. 1). A further indication that the original geochemical system is pristine is that all U–Th dates are in stratigraphic order (Fig. 1, Supplementary Fig. 2 and Supplementary Data 1).

If stalagmites are deposited under quasi-equilibrium conditions and diagenetic processes did not alter the original geochemical status, speleothem $\delta^{18}O$ ($\delta^{18}O_{sp}$) is principally inherited by rainfall $\delta^{18}O$ ($\delta^{18}O_{rw}$). Considering that on glacial/interglacial time scales global ice-volume changes modify seawater $\delta^{18}O$ (and thus $\delta^{18}O_{rw}$), SA1-$\delta^{18}O$ has been checked to evaluate this contribution according to other works[69]. However, the peculiar SA1-$\delta^{18}O$ pattern is still well recognisable after the correction for global ice-volume (Supplementary Fig. 7), meaning that other factors influenced $\delta^{18}O_{rw}$, and thus $\delta^{18}O_{sp}$. We have reasons to believe that SA1-$\delta^{18}O$ was controlled by the amount effect[42] combined with the uptake of moisture from two endmember-like sources, the Atlantic and the Mediterranean. Indeed, the primary role of the amount effect controlling $\delta^{18}O_{sp}$ in speleothems of the central and western Mediterranean realm has been indicated by other Mediterranean studies, for example along the Spanish Mediterranean borderlands[39] and islands[70], Croatia[71] and Macedonia[72]. In Italy, the same effect dominates $\delta^{18}O_{sp}$ in the northern and central portion of the Peninsula[32,67,73–77] and Sardinia[45,66]. Rainfall amount was also driving $\delta^{18}O_{sp}$ in the above-mentioned PC stalagmite[36] in a cave ~40 km NW with respect to Sant'Angelo (Supplementary Fig. 1). This is because air temperature and rainfall amount compete in modulating $\delta^{18}O_{rw}$ at central and western Mediterranean latitudes, but while rainfall amount and $\delta^{18}O_{rw}$ show a strongly negative gradient of $\sim -1.6‰ \times 100\ mm^{-1}$ rain, temperature and $\delta^{18}O_{rw}$ show a weakly positive gradient[78] of ~0.22% $°C^{-1}$. Additionally, laboratory[79] and in-situ[80] measurements reveal that during speleothem deposition the equilibrium water-calcite $\delta^{18}O$ fractionation ranges between −0.24‰ $°C^{-1}$ and −0.18‰ $°C^{-1}$; this makes the temperature-dependent isotope fractionation of atmospheric precipitation above the cave inefficient in driving $\delta^{18}O_{sp}$ with respect to the amount effect. Therefore, SA1-$\delta^{18}O$ primarily reflects palaeorainfall amount, with more negative $\delta^{18}O_{sp}$ indicating increased rainfall and vice versa.

There are other lines of evidence supporting that rainfall controlled SA1-$\delta^{18}O$. Rainfall variations should also affect the karst hydrology and thus the interaction between infiltrating water and bedrock. When rainfall decreases the groundwater residence time increases, leading to more efficient leaching of ^{234}U due to the alpha recoil effect[81] and resulting in higher $[^{234/238}U]_i$ ratios in speleothems. The opposite effect is expected during wet periods. At the same time, during wet periods carbonate deposition in caves is high and speleothem growth rate potentially increases. Besides the higher rainfall, increased temperature associated with humid periods promotes faster $CaCO_3$ deposition in the cave. The opposite is expected during relatively drier (and colder) periods, thus resulting in slower growth rates. A clear tendency towards lower (higher) $[^{234/238}U]_i$ when $\delta^{18}O$ values are shifted toward more (less) negative ones is visible in SA1 (Fig. 2 and Supplementary Fig. 6). Furthermore, growth rate maxima are mostly correlated with rapid SA1-$\delta^{18}O$ shifts toward more negative values. This ultimately highlights the same control for $[^{234/238}U]_i$, growth rate, and $\delta^{18}O$ in SA1, which is ultimately attributed to variation in rainfall amount.

For the reasons outlined above, we are confident that variations in rainfall amount controlled at least in part SA1-$\delta^{18}O$. According to Corchia Cave $\delta^{18}O$[32] in northern Italy, which reflects rainfall amount variability across T-II (Supplementary Fig. 8), rainfall changes in southern Italy during T-I were in turn driven by the strength of the westerlies delivering Atlantic moisture across the Mediterranean. The westerlies transport more moisture to the central Mediterranean area when the northern high-latitude ice sheets are small, and the AMOC is strong (as it is today), favouring the advection of moisture across Europe and the Mediterranean (Fig. 4[32]) In contrast, rainfall decreases when advection of moisture is reduced[32]. This occurs when the northern ice sheets expand and the AMOC weakens. Orbital parameters were similar during T-I and T-II with respect to obliquity and winter insolation[82] (Supplementary Fig. 8). Indeed, in the study area, obliquity has a major control on glacial terminations[83], while summer insolation has a minor effect. During T-I and T-II SA1-$\delta^{18}O$ and Corchia-$\delta^{18}O$ were coupled to $\delta^{18}O$ changes in planktonic foraminifera (G. bulloides) on the Iberian Margin[47] (Supplementary Fig. 8), further indicating that they share the same regional climate trigger during deglaciations.

Besides rainfall amount, another process is responsible in influencing SA1-$\delta^{18}O$. In agreement with Columbu et al. (2020)[36], the differential moisture uptake from the Atlantic and the Mediterranean was likely modulating SA1-$\delta^{18}O$. Today the Atlantic Ocean provides most of the rainfall to Apulia (Supplementary Fig. 4), while a smaller contribution is given by the Mediterranean Sea[84]. Atlantic rainfall $\delta^{18}O_{rw}$ is more negative than Mediterranean rainfall $\delta^{18}O_{rw}$, and the primary role of the Atlantic-sourced rainfall occurs if: (1) moisture produced in the Atlantic is abundant; and (2) westerlies efficiently delivers this moisture to the Mediterranean area. This signifies that when polar ice sheets expand, during colder-than-Holocene climate, the role of Atlantic-related moisture decreases in favour of Mediterranean-related moisture (Fig. 4). The opposite is expected if polar ice sheets shrink. The Atlantic vs Mediterranean source effect[42] generally mimics the Greenland T-I cyclicity if other effects are of minor importance. In central Mediterranean speleothems, this produces more negative $\delta^{18}O$ values during GI1 and the Holocene and less negative values during GS2 and GS1, as also found in the western side of the Mediterranean basin[24].

Data availability

The datasets generated and/or analysed in this study are available in Supplementary Data 1 and 2 and in the SISAL database https://doi.org/10.5194/essd-10-1687-2018.

Received: 30 May 2022; Accepted: 26 July 2022;
Published online: 17 August 2022

References

1. Buizert, C. et al. Greenland-wide seasonal temperatures during the last deglaciation. *Geophys. Res. Lett.* **45**, 1905–1914 (2018).
2. Tierney, J. E. et al. Glacial cooling and climate sensitivity revisited. *Nature* **584**, 569–573 (2020).
3. Clark, P. U. et al. Global climate evolution during the last deglaciation. *Proc. Natl Acad. Sci. USA* **109**, E1134–E1142 (2012).
4. Lambeck, K., Rouby, H., Purcell, A., Sun, Y. & Sambridge, M. Sea level and global ice volumes from the Last Glacial Maximum to the Holocene. *Proc. Natl Acad. Sci. USA* **111**, 15296–15303 (2014).
5. Mackintosh, A. et al. Retreat of the East Antarctic ice sheet during the last glacial termination. *Nature Geosci.* **4**, 195–202 (2011).
6. Dalton, A. S. et al. An updated radiocarbon-based ice margin chronology for the last deglaciation of the North American Ice Sheet Complex. *Quaternary Sci. Rev.* **234**, 106223 (2020).
7. Skinner, L. C., Fallon, S., Waelbroeck, C., Michel, E. & Barker, S. Ventilation of the deep Southern Ocean and deglacial CO_2 rise. *Science* **328**, 1147–1151 (2010).
8. Barker, S. et al. 800,000 years of abrupt climate variability. *Science* **334**, 347–351 (2011).
9. Muschitiello, F. et al. Deep-water circulation changes lead North Atlantic climate during deglaciation. *Nat. Commun.* **10**, 1–10 (2019).
10. North Greenland Ice Core Project (NGRIP) Members. High-resolution record of Northern Hemisphere climate extending into the last interglacial period. *Nature* **431**, 147–151 (2004).
11. Liu, Z. et al. Transient simulation of last deglaciation with a new mechanism for Bølling-Allerød warming. *Science* **325**, 310–314 (2009).
12. Buizert, C. et al. Greenland temperature response to climate forcing during the last deglaciation. *Science* **345**, 1177–1180 (2014).
13. Steffensen, J. P. et al. High-resolution Greenland ice core data show abrupt climate change happens in few years. *Science* **321**, 680–684 (2008).
14. Landais, A., Jouzel, J., Masson-Delmotte, V. & Caillon, N. Large temperature variations over rapid climatic events in Greenland: a method based on air isotopic measurements. *Comptes Rendus Geosci.* **337**, 947–956 (2005).
15. Rasmussen, S. O. et al. A stratigraphic framework for abrupt climatic changes during the Last Glacial period based on three synchronized Greenland

ice-core records: refining and extending the INTIMATE event stratigraphy. *Quaternary Sci. Rev.* **106**, 14–28 (2014).
16. Kindler, P. et al. Temperature reconstruction from 10 to 120 kyr b2k from the NGRIP ice core. *Clim. Past* **10**, 887–902 (2014).
17. Camuera, J. et al. Chronological control and centennial-scale climatic subdivisions of the Last Glacial Termination in the western Mediterranean region. *Quaternary Sci. Rev.* **255**, 106814 (2021).
18. Giorgi, F. Climate change hot-spots. *Geophys. Res. Lett.* **33**, L08707 (2006).
19. Brunetti, M., Buffoni, L., Mangianti, F., Maugeri, M. & Nanni, T. Temperature, precipitation and extreme events during the last century in Italy. *Global Planetary Change* **40**, 141–149 (2004).
20. Spano, D. et al. Analisi del rischio. I cambiamenti climatici in Italia. *Fondazione CMCC - Centro Euro-Mediterraneo sui Cambiamenti Climatici. Report* **2020**, 1–125 (2020).
21. Fink, A. et al. The 2003 European summer heatwaves and drought - synoptic diagnosis and impacts. *Weather* **54**, 209–216 (2004).
22. Bar-Matthews, M., Ayalon, A., Gilmour, M., Matthews, A. & Hawkesworth, C. J. Sea–land oxygen isotopic relationships from planktonic foraminifera and speleothems in the Eastern Mediterranean region and their implication for paleorainfall during interglacial intervals. *Geochimica et Cosmochimica Acta* **67**, 3181–3199 (2003).
23. Badertscher, S. et al. Pleistocene water intrusions from the Mediterranean and Caspian seas into the Black Sea. *Nat. Geosci.* **4**, 236–239 (2011).
24. García-Alix, A. et al. Paleohydrological dynamics in the Western Mediterranean during the last glacial cycle. *Glob. Planetary Change* **202**, 103527 (2021).
25. Lechleitner, F. et al. The potential of speleothems from Western Europe as recorders of regional climate: a critical assessment of the SISAL Database. *Quaternary* **1**, 1–31 (2018).
26. Allen, J. R. M. et al. Rapid environmental changes in southern Europe during the last glacial period. *Science* **400**, 740–743 (1999).
27. Tzedakis, P. C., Hooghiemstra, H. & Pälike, H. The last 1.35 million years at Tenaghi Philippon: revised chronostratigraphy and long-term vegetation trends. *Quaternary Sci. Rev.* **25**, 3416–3430 (2006).
28. Lionello, P., Malanotte-Rizzoli, P. & Boscolo, R. Mediterranean climate variability. *Dev. Earth Environ. Sci.* **4**, 421 (2006).
29. Guiot, J. & Cramer, W. Climate change: the 2015 Paris Agreement thresholds and Mediterranean basin ecosystems. *Science* **354**, 465–468 (2016).
30. Wagner, B. et al. Mediterranean winter rainfall in phase with African monsoons during the past 1.36 million years. *Nature* **573**, 256–260 (2019).
31. Sánchez Goñi, M. F., Eynaud, F., Turon, J. L. & Shackleton, N. J. High resolution palynological record off the Iberian margin: direct land-sea correlation for the Last Interglacial complex. *Earth Planet. Sci. Lett.***171**, 123–137 (1999).
32. Drysdale, R. N. et al. Evidence for obliquity forcing of glacial Termination II. *Science* **325**, 1527–1531 (2009).
33. Cheng, H. et al. The climatic cyclicity in semiarid-arid central Asia over the past 500,000 years. *Geophys. Res. Lett.* **39**, 1 (2012).
34. Dixit, Y. et al. Enhanced western mediterranean rainfall during past interglacials driven by North Atlantic pressure changes. *Quaternary Int.* **553**, 1–13 (2020).
35. Lionello, P. The climate of the Mediterranean region: from the past to the future. Elsevier, 2012.
36. Columbu, A. et al. Speleothem record attests to stable environmental conditions during Neanderthal-Modern Human turnover in Southern Italy. *Nat. Ecol. Evolut.* **4**, 1188–1195 (2020).
37. Zielhofer, C. et al. Atlantic forcing of Western Mediterranean winter rain minima during the last 12,000 years. *Quaternary Sci. Rev.* **157**, 29–51 (2017).
38. Toney, J. L. et al. New insights into Holocene hydrology and temperature from lipid biomarkers in western Mediterranean alpine wetlands. *Quaternary Sci. Rev.* **240**, 106395 (2020).
39. Budsky, A. et al. Western Mediterranean climate response to Dansgaard/Oeschger events: new insights from speleothem records. *Geophys. Res. Lett.* **46**, 9042 (2019).
40. Rogerson, M. et al. Enhanced Mediterranean water cycle explains increased humidity during MIS 3 in North Africa. *Climate of the Past* **15**, 1757–1769 (2019).
41. Breitenbach, S. F. M. et al. COnstructing proxy-record age models (COPRA). *Climate of the Past.* **8**, 1765–1779 (2012).
42. Dansgaard, W. Stable isotopes in precipitation. *Tellus* **16**, 436–468 (1964).
43. Moreno, A. et al. Climate controls on rainfall isotopes and their effects on cave drip water and speleothem growth: the case of Molinos cave (Teruel, NE Spain). *Climate Dynamics* **43**, 221–241 (2014).
44. Bernal-Wormull, J. L. et al. Immediate temperature response in northern Iberia to last deglacial changes in the North Atlantic. *Geology* no. **49**, 999–1003 (2021).
45. Columbu, A. et al. A long record of MIS 7 and MIS 5 climate and environment from a western Mediterranean speleothem (SW Sardinia, Italy). *Quaternary Sci. Rev.* **220**, 230–243 (2019).
46. Eynaud, F. et al. New constraints on European glacial freshwater releases to the North Atlantic Ocean. *Geophys. Res. Lett.* **39**, 15 (2012).
47. Martrat, B. et al. Four climate cycles of recurring deep and surface water destabilizations on the Iberian margin. *Science* **317**, 502–507 (2007).
48. Toucanne, S. et al. Tracking rainfall in the northern Mediterranean borderlands during sapropel deposition. *Quaternary Sci. Rev.* **129**, 178–195 (2015).
49. Grant, K. M. et al. Rapid coupling between ice volume and polar temperature over the past 150,000 years. *Nature* **491**, 744–747 (2012).
50. Darfeuil, S. et al. Sea surface temperature reconstructions over the last 70 kyr off Portugal: Biomarker data and regional modeling. *Paleoceanography* **31**, 40–65 (2016).
51. Siani, G., Magny, M., Paterne, M., Debret, M. & Fontugne, M. Paleohydrology reconstruction and Holocene climate variability in the South Adriatic Sea. *Clim. Past* **9**, 499–515 (2013).
52. Affolter, S. et al. Central Europe temperature constrained by speleothem fluid inclusion water isotopes over the past 14,000 years. *Sci. Adv.* **5**, 6 (2019).
53. von Grafenstein, U., Erlenkeuser, H., Brauer, A., Jouzel, J. & Johnsen, S. J. A mid-European decadal isotope-climate record from 15,500 to 5000 years BP. *Science* **284**, 1654–1657 (1999).
54. Cheng, H. et al. Timing and structure of the Younger Dryas event and its underlying climate dynamics. *Proc. Natl Acad. Sci. USA* **117**, 23408–23417 (2020).
55. Luetscher, M. et al. North Atlantic storm track changes during the Last Glacial Maximum recorded by Alpine speleothems. *Nat. Commun.* **6**, 6344 (2015).
56. Camuera, J. et al. Quantitative reconstruction of hydroclimate variability over the last 200 kyr in the West Mediterranean. *PANGAEA* https://doi.org/10.1594/PANGAEA.940006 (2022).
57. IPCC, 2021, Climate Change 2021: The Physical Science Basis. Contribution of Working Group I to the Sixth Assessment Report of the Intergovernmental Panel on Climate Change [Masson-Delmotte, V., et al. (eds.)]. Cambridge University Press. In Press.
58. Drysdale, R. et al. Magnesium in subaqueous speleothems as a potential palaeotemperature proxy: Nature. *Nat. Commun.* **11**, 1–11 (2020).
59. Shen, C.-C. et al. High-precision and high-resolution carbonate 230Th dating by MC-ICP-MS with SEM protocols. *Geochim. Cosmochim. Acta* **99**, 71–86 (2012).
60. Hendy, C. H. The isotopic geochemistry of speleothems-I. The calculation of the effects of different modes of formation on the isotopic composition of speleothems and their applicability as palaeoclimatic indicators. *Geochim. Cosmochim. Acta* **35**, 801–824 (1971).
61. Fairchild, I. J. and Baker, A., 2012, Speleothem science: from process to past environments: John Wiley & Sons, Chichester.
62. Dorale, J. A. & Liu, Z. Limitations of hendy test criteria in judging the paleoclimatic suitability of speleothems and the need for replication. *J. Cave and Karst Stud.* **71**, 73–80 (2009).
63. Daeron, M. et al. Most Earth-surface calcites precipitate out of isotopic equilibrium. *Nat. Commun.* **10**, 429 (2019).
64. Mickler, P. J., Stern, L. A. & Banner, J. L. Large kinetic isotope effects in modern speleothems. *Geol. Soc. Am. Bull.* **118**, 65–81 (2006).
65. Fairchild, I. J. et al. Modification and preservation of environmental signals in speleothems. *Earth-Sci. Rev.* **75**, 105–153 (2006).
66. Columbu, A. et al. Early last glacial intra-interstadial climate variability recorded in a Sardinian speleothem. *Quaternary Sci. Rev.* **169**, 391–397 (2017).
67. Columbu, A., Sauro, F., Lundberg, J., Drysdale, R. & De Waele, J. Palaeoenvironmental changes recorded by speleothems of the southern Alps (Piani Eterni, Belluno, Italy) during four interglacial to glacial climate transitions. *Quaternary Sci. Rev.* **197**, 319–335 (2018).
68. Bajo, P. et al. "Cryptic" diagenesis and its implications for speleothem geochronologies. *Quaternary Sci. Rev.* **148**, 17–28 (2016).
69. Bintanja, R., van de Wal, R. S. & Oerlemans, J. Modelled atmospheric temperatures and global sea levels over the past million years. *Nature* **437**, 125–128 (2005).
70. Dumitru, O. A. et al. Climate variability in the western Mediterranean between 121 and 67 ka derived from a Mallorcan speleothem record. *Palaeogeogr. Palaeoclimatol. Palaeoecol.* **506**, 128–138 (2018).
71. Surić, M. et al. Holocene hydroclimate changes in continental Croatia recorded in speleothem δ13C and δ18O from Nova Grgosova Cave. *The Holocene* **31**, 1401–1416 (2021).
72. Regattieri, E. et al. A MIS 9/MIS 8 speleothem record of hydrological variability from Macedonia (F.Y.R.O.M.). *Global and Planetary Change* **162**, 39–52 (2018).
73. Regattieri, E. et al. Interstadial conditions over the Southern Alps during the early penultimate glacial (MIS 6): a multiproxy record from Rio Martino Cave (Italy). *Quaternary Sci. Rev.* **257**, 106856 (2021).

74. Regattieri, E. et al. A continuous stable isotope record from the penultimate glacial maximum to the Last Interglacial (159–121ka) from Tana Che Urla Cave (Apuan Alps, central Italy). *Quaternary Res.* **82**, 450–461 (2014).
75. Regattieri, E. et al. Holocene Critical Zone dynamics in an Alpine catchment inferred from a speleothem multiproxy record: disentangling climate and human influences. *Scientific Rep.* **9**, 17829 (2019).
76. Vanghi, V. et al. Climate variability on the Adriatic seaboard during the last glacial inception and MIS 5c from Frasassi Cave stalagmite record. *Quaternary Sci. Rev.* **201**, 349–361 (2018).
77. Zanchetta, G. et al. Beyond one-way determinism: San Frediano's miracle and climate change in Central and Northern Italy in late antiquity. *Clim. Change* **165**, 1–21 (2021).
78. Bard, E. et al. Hydrological conditions over the western Mediterranean basin during the deposition of the cold Sapropel 6 (ca. 175 Kyr BP). *Earth Planet. Sci. Lett.* **202**, 481–494 (2002).
79. Kim, S.-T. & O'Neil, J. R. Equilibrium and nonequilibrium oxygen isotope effects in synthetic carbonates. *Geochim. Cosmochim. Acta* **61**, 3461–3475 (1997).
80. Tremaine, D. M., Froelich, P. N. & Wang, Y. Speleothem calcite farmed in situ: Modern calibration of $\delta^{18}O$ and $\delta^{13}C$ paleoclimate proxies in a continuously-monitored natural cave system. *Geochim. Cosmochim. Acta* **75**, 4929–4950 (2011).
81. Drysdale, R. N., Zanchetta, G., Hellstrom, J., Fallick, A. E. & Zhao, J. Stalagmite evidence for the onset of the Last Interglacial in southern Europe at 129 ± 1 ka. *Geophys. Res. Lett.* **32**, L24708 (2005).
82. Berger, A. & Loutre, M. F. Insolation values for the climate of the last 10 million years. *Quaternary Sci. Rev.* **10**, 297–317 (1991).
83. Bajo, P. et al. Persistent influence of obliquity on ice age terminations since the Middle Pleistocene transition. *Science* **367**, 1235–1239 (2020).
84. Longinelli, A. & Selmo, E. Isotopic composition of precipitation in Italy: a first overall map. *J. Hydrol.* **270**, 75–88 (2003).

Acknowledgements

U-Th dating at the High-Precision Mass Spectrometry and Environment Change Laboratory (HISPEC) was supported by grants from the Science Vanguard Research Program of the Ministry of Science and Technology (MOST), Taiwan, ROC (110-2123-M-002-009 to C.-C.S.), the Higher Education Sprout Project of the Ministry of Education, Taiwan, ROC (110L901001 to C.-C.S.), the National Taiwan University (110L8907 to C.-C.S.). Sampling of speleothems was allowed by the local administration. We thank all local speleologists that helped during fieldwork. We finally thank three anonymous reviewers for their insightful comments.

Author contributions

Columbu conceived the project, designed the experiments (after preliminary experiments by Chiarini), analysed and interpreted the data, created the images and wrote the paper; all these activities were accomplished with contributions from all co-authors. Columbu, Fohlmeister, Chiarini, Spötl, Hellstrom, Cheng, Hu and Shen performed experiments and/or data analyses. Columbu, Chiarini and De Waele participated in the fieldwork.

Competing interests

The authors declare no competing interests.

Additional information

Supplementary information The online version contains supplementary material available at https://doi.org/10.1038/s43247-022-00509-3.

Correspondence and requests for materials should be addressed to Andrea Columbu.

Peer review information *Communications Earth & Environment* thanks the anonymous reviewers for their contribution to the peer review of this work. Primary Handling Editor: Joe Aslin.

Reprints and permission information is available at http://www.nature.com/reprints

Publisher's note Springer Nature remains neutral with regard to jurisdictional claims in published maps and institutional affiliations.